A new version of the SWIFT platform for waves, currents, and turbulence in the ocean surface layer

Jim Thomson
Applied Physics Laboratory
University of Washington
Seattle WA, USA
jthomson@apl.uw.edu

Melissa Moulton
Applied Physics Laboratory
University of Washington
Seattle WA, USA
mmoulton@apl.uw.edu

Alex de Klerk
Applied Physics Laboratory
University of Washington
Seattle WA, USA
adeklerk@apl.uw.edu

Joe Talbert
Applied Physics Laboratory
University of Washington
Seattle WA, USA
jtalbert@apl.uw.edu

Maricarmen Guerra
Dept. of Oceanography
Dalhousie University
Halifax, NS, Canada
MGuerra@dal.ca

Sam Kastner
Dept. of Civil and Environmental Engineering
University of Washington
Seattle WA, USA
skastner@uw.edu

Madison Smith
Dept. of Civil and Environmental Engineering
University of Washington
Seattle WA, USA
mmsmith@apl.uw.edu

Mike Schwendeman
Applied Physics Laboratory
University of Washington
Seattle WA, USA
schwendeman.mike@gmail.com

Seth Zippel
Applied Ocean Physics and Eng.
Woods Hole Oceanographic Inst.
Woods Hole MA, USA
zippelsf@whoi.edu

Sven Nylund
Nortek, Inc
Rud, Norway
Sven.Nylund@nortekgroup.com

***Abstract*—The Surface Wave Instrument Float with Tracking (SWIFT) is a freely drifting platform for measurements of waves, currents, and turbulence in the ocean surface layer. This platform has been used globally to study wave breaking, wave-current interactions, and waves in ice. A new version (v4) of the buoy has recently been developed and demonstrated in the Office of Naval Research "Langmuir Circulations" field campaign along the California coast (2017). The new version is built around a 5-beam Acoustic Doppler Current Profiler (Nortek Signature 1000) with a multi-pulse coherent mode for high-resolution turbulence measurements. The new Doppler profiler enables estimates of the turbulent dissipation rate down to 3.5 m below waves, compared with 0.5 m in the previous version, and can measure a much larger range of turbulence levels than the previous version. The new version also uses a broadband Doppler mode to profile the mean currents down to 20 m. Mean Eulerian velocity profiles are estimated from the wave-averaged profiler velocities by applying a wave-following bias correction that scales with the Stokes drift and has twice the vertical decay scale. Finally, the new version supports real-time telemetry of raw sea surface elevations for reconstruction of individual waves by processing a coherent array of multiple SWIFTs, with applications for short-range wave-by-wave forecasting. These combined improvements to the platform are intended to advance understanding of wave processes and applications in the ocean surface layer.**

***Index Terms*—Ocean, surface, wave, currents, turbulence, buoy**

I. Introduction

The original Surface Wave Instrument Float with Tracking (SWIFT) was developed in 2009 with the goal of measuring turbulence within breaking ocean surface waves [1]. The buoys drift freely at the ocean surface and collect measurements in a wave following reference frame. The production version (v3) was developed in 2013, using a spar-like hull shape (1.2 m draft, 0.3 m diameter) to accommodate the Nortek AquadoppHR profiler. Approximately 20 SWIFT v3 buoys have been produced and are in regular use. They have been used to measure near-surface turbulent dissipation rates in a variety of environments [2]–[6].

A new version (v4) of the SWIFT platform was recently developed, and four units have been produced. The new version is built around the Nortek Signature 1000 Doppler profiler, which has several advantages over the AquadoppHR used on earlier versions. Most importantly, the Signature 1000 has a lower noise level in the velocity estimates. The Signature 1000 also supports concurrent measurements in high resolution (HR) mode on the vertical beam with broadband (BB) mode on the four divergent beams. The new capabilities highlight the importance of correcting the wave-bias in the observed current profiles. Another improvement described herein is availability of real-time wave data for phase-resolved wave projections.

A. Buoy Specifications

The v4 SWIFT is smaller and has a shallower draft, without the spar-like hull of earlier versions. The weight in air is 20 kg, and the net buoyancy is 12 kg. The maximum diameter is 0.45 m, the total height is 0.52 m, and the draft is 0.25 m.

The Nortek Signature1000 is mounted downlooking in the center of the hull, as shown in Figure 1. The Signature head

Support provided by the Office of Naval Research.

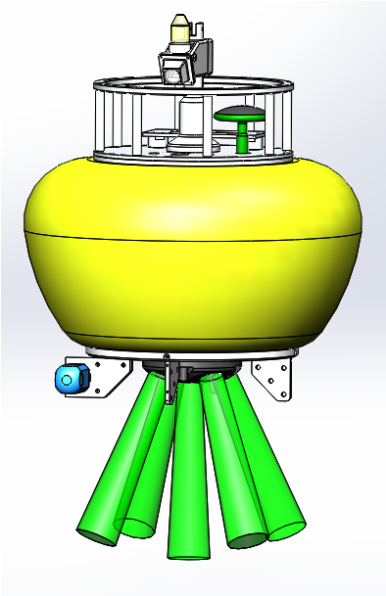

Fig. 1. SWIFT v4. The green cylinders indicate the Signature1000 beam pattern, and the yellow hull is the flotation collar.

TABLE I
SWIFT V4 SPECIFICATIONS

Payload	Purpose	Configuration
Sutron Expert	Data processing	C++ libraries
uCam	Surface images	0.5 Hz
SBG Ellipse N	Waves	5 Hz heave, GPS/GNSS
Nortek Signature1000 (HR)	Turbulence profiles	96 bins (0.04 m), 8 Hz
Nortek Signature1000 (BB)	Current profiles	40 bins (0.5 m), 1 Hz
Aanderaa 4319	Conductivity	0.5 Hz
Aanderaa 4319	Temperature	0.5 Hz
Airmar WX200	Winds	4 Hz
Digi XPress Ethernet Bridge	Realtime data	RF radio (900 MHz)
Iridium modem	Data telemetry	hourly bulk parameters
AIS beacon	Tracking	2 min update

is integrated into a custom pressure case, which also houses the Sutron Xpert data logger and processing board, as well as an Iridium modem and SBG Ellipse inertial navigation system (INS). The lower hull has several expansion ports; to date, these have been configured for: a conductivity and temperature probe, an oxygen optode, and a fluorometer. Table I summarizes the sensor payloads and sampling details.

Data are collected onboard the buoy in bursts lasting 512 s, at an interval of 720 s (i.e., 5 bursts per hour). The 208 s between each data collection are used for onboard processing of the Signature data and the SBG data (for wave spectra). The results are transmitted to shore using the Iridium SBD (short burst data) protocol, which has global coverage.

B. Langmuir Circulation Experiment (2017)

The Langmuir Circulation Experiment was conducted off of Southern California in Spring 2017 as a collaborative Department Research Initiative (DRI) funded by the Office of Naval Research. SWIFTs were deployed from the R/V Sproul repeatedly from 19 March to 6 April, 2017, in a region to the east of Catalina Island. A total of eight SWIFT drifters were

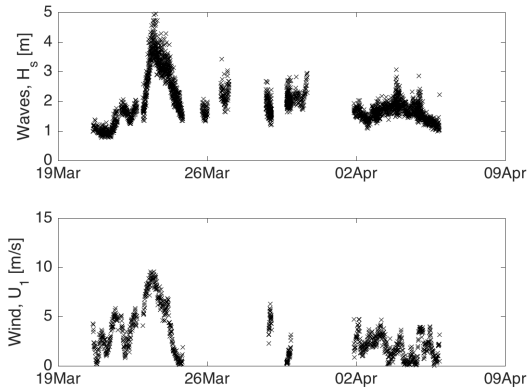

Fig. 2. Significant wave heights and wind speed during the Langmuir Circulation experiment (2017).

used: four older v3 models, and four new v4 models. Figure 2 shows the wave and wind conditions during the experiment, as measured by all eight SWIFTs. The v4 models deployed were serial numbers 22, 23, 24, and 25.

II. TURBULENT DISSIPATION RATE PROFILES

The structure function method [7] is used to process Signature profiles collected with the v4 SWIFTs, following the approach used to process AquadoppHR turbulence profiles collected with the v3 SWIFTs. These profiles use only the 5th beam of the Signature, collected in HR mode with 96 bins at 0.04 m resolution and at 8 Hz sampling rate. The HR mode uses a multi-pulse coherent method to extend the velocity range [8], [9].

The structure function is the covariance of the difference in turbulent velocity u' between two points $\mathbf{z}+\mathbf{r}$ and $\mathbf{z}$,

$$D(z,r) = \overline{(u'(z+r) - u'(z))^2}. \tag{1}$$

When collected in the wave-following reference frame, wave orbital velocities are removed as a mean profile and z is relative to the instantaneous surface. If used in a fixed reference frame, the variance of the wave orbital velocities must be removed [10].

Assuming locally isotropic turbulence and $\eta_K \ll r \ll L$ where η_K is the Kolmogorov length scale and L is the largest eddy size (inertial subrange), the structure function has the form $D(z,r) = A(z)r^{2/3} + N$ and depth-dependent turbulence dissipation rates $\epsilon(z,t)$ can be estimated as

$$\epsilon(z,t) = \left(\frac{A(z,t)}{C}\right)^{3/2}, \tag{2}$$

where $A(z)$ is obtained by fitting a linear model $A(z)r^{2/3} + N$ to the time-averaged $D(z,r)$ at each z level and $C \sim 2$ is a universal constant. Here, N is an offset resulting from Doppler noise in the velocity measurements and the range of scales considered is 0.04 m $< r <$ 0.24 m (i.e., six HR bins to either side of a given position in the HR profile). Recently, [11] showed that these calculations can use very short temporal

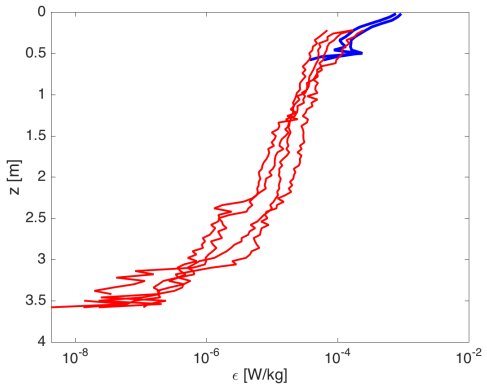

Fig. 3. Comparison of the turbulent dissipation rates profiles obtained from SWIFT buoys. The profile from the new v4 (red lines) is a deeper turbulence measurement with a lower noise floor, relative to the profile from the v3 (blue lines). There were four v4 and two v3 buoys near each other for these coincident measurements.

averages (i.e., the overbar in Eq. 1) and thereby examine phase resolved turbulence dissipation rates beneath individual waves.

Figure 3 shows example profiles collected with v3 and v4 SWIFTs near each other. The v4 profiles are much deeper (3.5 m versus 0.5 m), although they miss the shallowest depths where wave-breaking turbulence is the strongest. The v4 profiles have much larger dynamic range, which is expected as a result of the lower noise in the turbulent velocity measurements. Based on the a priori estimates of velocity noise, $\sigma < 0.01$ m/s, and the noise intercept $N = 2\sigma^2$ to the structure function fits, the v4 profiles should be capable of measuring dissipation rates as small as $10^{-8}m^2/s^3$. This is notable improvement over the limit of $10^{-5}m^2/s^3$ for the v3.

III. Current Profiles

Accurate measurements of velocity and shear are important for understanding upper-ocean dynamics, including the relative importance of breaking-wave-driven mixing and shear-driven turbulence. Drifting platforms such as SWIFTs collect measurements of mean (wave-averaged) current profiles that are biased as a result of wave motions. The bias results from a phase-coupling of the position of velocity profiler measurement bins and the vertically decaying Eulerian surface-gravity-wave velocity field [12]–[16]. For surface-drifting platforms, the bias in the absolute velocity scales with the Stokes drift surface velocity, with a vertical decay lengthscale that is twice that of the Stokes drift. This wave-following bias can be applied as a correction to estimate Eulerian velocities [16].

A. Wave-following bias

Measurement bins of the downward-looking Signature1000 on the SWIFT v4 move in trajectories with the same shape as the surface-wave-following drifter motion, with a vertical offset or distance to each bin Δz. Thus, the mean (wave-averaged) velocity estimated in each bin is neither a Lagrangian nor Eulerian measurement. The profiler samples larger positive velocities (in the wave direction) when a bin is at the top of an orbit, and smaller negative velocities (opposite the wave direction) when the bin is at the bottom of an orbit. Thus, over a wave cycle, the velocity sampled in each profiler bin averages to a positive value (in the wave direction). This net wave-averaged velocity has similar kinematics to the Stokes drift, and is equal to the Stokes drift at the profiler elevation. For a profiler with vertical position Z_0 in a water column with depth h in a monochromatic wave field with height a, angular frequency ω and wavenumber k, the wave-following bias in a profiler bin at $z = Z_0 + \Delta z$ (with offset Δz from the platform) is

$$\tilde{u}(z) = a^2\omega k \frac{\cosh[2k(Z_0+h)+k\Delta z]}{2\sinh^2(kh)} \tag{3}$$

Note that this expression is the same as Equation (10) in Amador et al., 2017 [16], except that a typo has been corrected in the vertical decay scale.

Similar to the Stokes drift, the wave-following bias velocity components $\tilde{u}(z), \tilde{v}(z)$ can be estimated with bulk wave properties. However, more accurate estimates can be made using additional frequency-direction spectral information [17], [18]. For a surface following float with $Z_0 = 0$, in a monochromatic unidirectional wave field with significant wave height H_s, bulk wavenumber k, radian frequency ω, and mean direction θ (geographic angle, direction from, clockwise relative to north),

$$(\tilde{u}(z), \tilde{v}(z)) = \frac{H_s^2}{16}\omega k \frac{\cosh(kz+2kh)}{\sinh^2(kh)}(\sin\theta, \cos\theta) \tag{4}$$

Given a frequency spectrum $S_{\eta\eta}(f)$ and the first-moment normalized directional Fourier coefficients, a_1 and b_1, the bias can be estimated as:

$$(\tilde{u}(z), \tilde{v}(z)) = \int S_{\eta\eta}(f)\omega k \frac{\cosh(kz+2kh)}{\sinh^2(kh)}(-a_1, -b_1)df \tag{5}$$

Here, the scalar spectra $S_{\eta\eta}(f)$ and directional moments are determined onboard the SWIFTs by processing motion data [1], [19], [20].

Alternatively, the bias can be estimated by integrating over a frequency-direction spectrum ($S_{\eta\eta}(f,\theta)$):

$$(\tilde{u}(z), \tilde{v}(z)) = \iint S_{\eta\eta}(f,\theta)\omega k \frac{\cosh(kz+2kh)}{\sinh^2(kh)}(\sin\theta, \cos\theta)df\,d\theta \tag{6}$$

The spectrum $S_{\eta\eta}(f,\theta)$ can be estimated from measurements using a directional estimator (e.g., MEM, MLM) that uses a frequency spectrum $S_{\eta\eta}(f)$, the first four directional Fourier coefficients, and assumptions about higher order moments. Depending on the assumptions of the estimator, the results of Equation 6 may be the same as those of Equation 5. Equation 6 could also be used with a modeled wave spectrum, which would explicitly resolve the full directional distribution $S_{\eta\eta}(f,\theta)$.

For comparison, the Stokes drift is given by:

$$(u_s(z), v_s(z)) = \iint S_{\eta\eta}(f,\theta)\omega k \frac{\cosh[2k(z+h)]}{\sinh^2(kh)}(\sin\theta, \cos\theta)df\,d\theta \tag{7}$$

For typical wind seas, the bulk estimate is expected to overestimate the magnitude of the bias by 50-100% relative to the frequency-direction spectral estimate [18], and the inclusion of higher frequency waves in the frequency-direction spectral estimates leads to larger near-surface shear in the bias correction.

B. Corrected estimates of Eulerian velocity and shear

To estimate the Eulerian velocity components, $u_E(z), v_E(z)$, the velocity observed relative to the profiler is summed with a measured drift velocity, and the wave-following bias is is removed:

$$u_E(z) = u_m(z) + u_d - \tilde{u}(z) \tag{8}$$

$$v_E(z) = v_m(z) + v_d - \tilde{v}(z) \tag{9}$$

where $u_m(z), v_m(z)$ are the measured wave-averaged velocity components, u_d, v_d are the mean horizontal velocity components of the drifter measured with GPS/GNSS, and $\tilde{u}(z), \tilde{v}(z)$ (Equation 6) are the apparent velocity components resulting from wave-induced orbits of the profiler bins. The drift velocity is a result of both surface Stokes drift and the Eulerian surface current (wind-drag effects are small).

Here, Eulerian velocity profiles are estimated for the LCDRI dataset. For each SWIFT burst, the measured wave spectrum (Figure 4a) and first pair of Fourier moments (Figure 4b) are used to estimate the wave-following bias profile (Equation 6) (4d, red curve). The profiler velocity profile is summed with a measured drift to obtain a raw (uncorrected) absolute Eulerian velocity estimate (Figure 4d, blue curve), and a corrected estimate is obtained by removing the bias (Equations 8-9) (4d, cyan curve). In this example, applying the correction significantly changes the estimates of velocity and shear: the apparent eastward surface velocity is explained by the surface value of the wave-following bias (equal to the surface Stokes drift), and near-surface shear is reduced after removing the bias.

Figure 5 shows histograms of velocity corrections from the entire Langmuir Circulation experiment, spanning the conditions in Figure 2. In general, the wave bias corrections are small (< 0.05 m/s), relative to the observed magnitudes (up to 0.5 m/s). The corrections are largest within 5 m of the surface, as expected given the steep vertical dependence of the wave bias. Distributions of the sign of the velocity and shear corrections are relatively symmetric, suggesting that ignoring the bias can lead to either an over or under-estimate of near-surface velocity and shear. The distributions have a small skewness towards reducing the velocity and shear magnitude (ignoring the bias leads to overestimates of velocity magnitude and shear), consistent with the presence of larger velocity and shear in the wave direction.

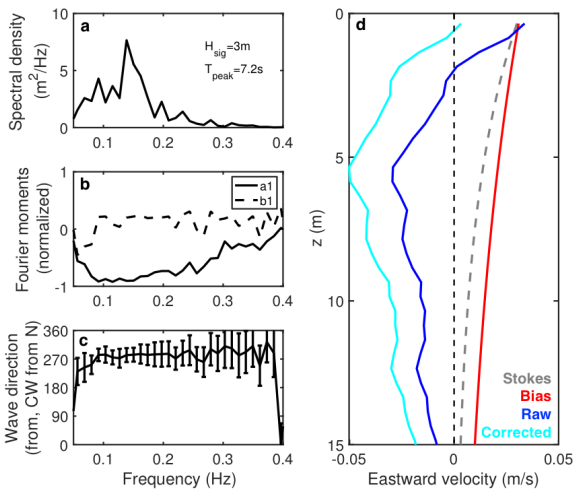

Fig. 4. (a) Measured wave spectrum, (b) first pair of directional moments, and (c) wave direction (curve) and spread (errorbars) versus frequency, and (d) eastward components (approximately in the wave direction) of Stokes drift (gray), wave-following bias (red), raw absolute profile (blue), and velocity with bias removed (cyan) versus distance from mean water surface.

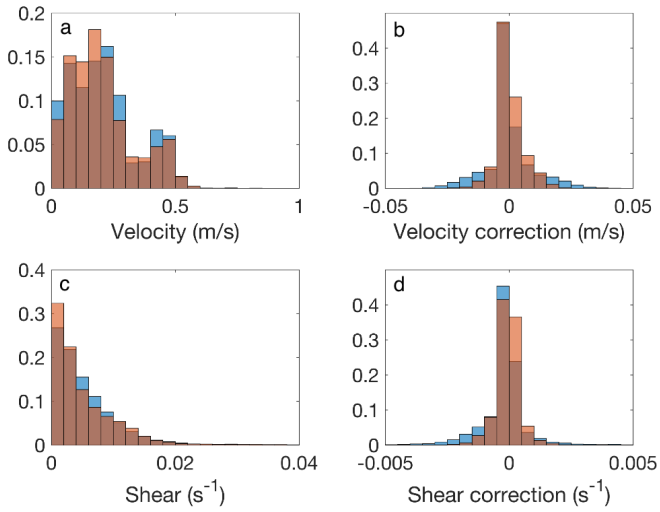

Fig. 5. Histograms of (a) velocity magnitude, (b) velocity magnitude correction, (c) Eulerian shear, and (d) shear correction for top 5 m of water column (blue) and at 5-15 m depth (orange).

IV. Phase-Resolved Wave Projection

Each of v4 SWIFTs include an ethernet bridge to broadcast raw wave motions in realtime, with a goal to integrate realtime data from a sparse array of buoys to make projections of individual waves a short amount of time or space into the future. Applications for such projections include ship maneuvering and optimization of wave energy conversion devices. One demonstrated approach to this problem is based on a least squares fit of the measurements to a sum of plane waves, which are then propagated forward in time by assuming linear dispersion [21]. Given enough observations and minimal nonlinearity, this method yields an accurate time domain, phase-resolved forecast of the approaching waves. This was developed for a coherent Doppler radar system, which has much larger spatial coverage and higher spatial resolution than an array of four buoys [21]. However, the radar can only estimate the radial wave orbital velocity, rather than surface

elevation, which the buoys do readily.

The algorithm is based around the representation of the sea surface as a sum of individual wave components, as in

$$\eta(\mathbf{x},t) = \Re\left(\sum_{n=1}^{N} A_n \exp(i(\mathbf{x}\cdot\mathbf{k}_n - \omega_n t))\right) \tag{10}$$

where A_n, $\mathbf{k}_n$, and ω_n are the amplitude, wavenumber, and frequency of each component. Assuming linear dispersion and deep water conditions, $\omega = \sqrt{gk}$, where g is gravitational acceleration and $k = \sqrt{k_x^2 + k_y^2}$.

The algorithm can be expressed in matrix form as

$$\eta = \mathbf{PA} \tag{11}$$

where $\mathbf{P}$ is an $N \times M$ matrix with elements

$$P_{n,m} = \exp(i(\mathbf{x}_m \cdot \mathbf{k}_n - \omega_n t_m)), \tag{12}$$

called the propagator matrix. η is an $M \times 1$ vector of observations, and $\mathbf{A}$ is an $N \times 1$ vector of unknown wave amplitudes. If $M > N$, this is an overdetermined system of equations, such that $\mathbf{A}$ can be fit using the linear least squares method. With the component amplitudes determined in this way, the surface elevation at a desired time and place can be projected using equation 10.

An example of the SWIFT processing is shown from 2 April, in which the SWIFT v4s were deployed in a square array with approximately 100 m spacing and drifted together for more than two hours. Conditions were $H_s \sim 2$ m from the west at $T_p \sim 12$ s. The SWIFTs drifted southeast together at approximately 0.25 m/s, with SWIFT 22 the farthest downwave. Thus, a test projection is made using data from SWIFTs 23, 24, and 25 to hindcast the waves at SWIFT 22. As the buoys are quite close together (< 100 meters), no delay is imposed and the prediction window is set to 5 seconds. For the 5 Hz wave data from three buoys, the algorithm runtime on a generic laptop is 0.2 seconds per 5 second burst.

The resulting prediction at SWIFT 22 is shown in Figure 6. The correlation of the two time series is $R^2 = 0.67$. The prediction captures many of the larger motions, though there is a fair amount of high frequency energy that is not represented well. This is perhaps to be expected, as the high frequency waves have less coherence over wide distances on the scale of the buoy separation. The predictions work best on large, long waves.

In the future, it may be possible to constrain the least squares fit to replicate the directional spectrum and thereby supplement the sparseness of the buoy array. One issue is the lack of continuity between prediction windows, even with overlapping data, and how this time windowing should work operationally. Ideally, the algorithm would be modified to be a rolling prediction, where each point is predicted from its own optimal window of observations. There may be an efficient way to program this to be incremental, using Kalman filters or another method, such that the calculations from the previous prediction are not discarded, and each new observation timestep yields one new prediction, and adds only a small additional computation. Finally, it may be that there are simpler projections than the full time series of predicted surface elevation that are useful for applications. A simple warning of an imminent large wave may be useful, relative to the purely statistical wave forecasts presently available.

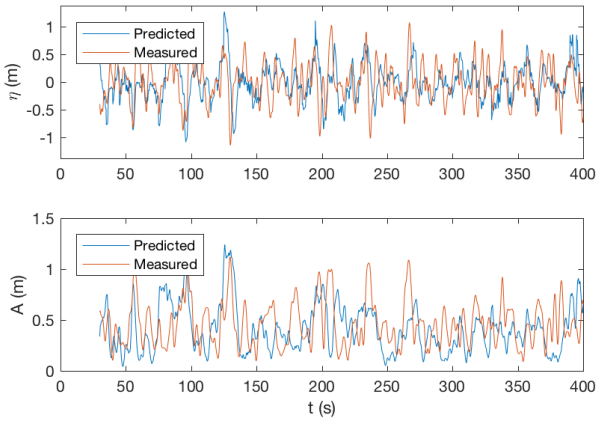

Fig. 6. Comparison of predicted and measured surface elevation η, and wave envelope A, at SWIFT 22.

V. Discussion and Conclusions

The latest version (v4) of the SWIFT buoy has been developed and includes the following advantages relative to earlier versions:

- Deeper profiles of turbulent dissipation rates covering a wider dynamic range
- Current profiles corrected for wave biases
- Realtime wave data for phase-resolved wave projections

These new capabilities are intended to assess basic research questions regarding turbulence in the ocean surface layer. The structure of bubble plumes and diffusion of turbulence after wave breaking remain active areas for research. Likewise, wind-wave-current relationships including combined Stokes-Coriolis and Ekman dynamics, and the relative importance of Eulerian and Lagrangian shear including generation of Langmuir turbulence, continue to require observations that can constrain models [22], [23].

More information, including deployment data, can be found at www.apl.uw.edu/SWIFT. The codes used in data processing are publicly available at https://github.com/jthomson-apluw/SWIFT-codes.

Acknowledgment

Thanks to the R/V Sproul for deployments and recoveries. Thanks to Eric D'Asaro, Andrey Shcherbina, Mike Ohmart (all APL-UW) for support during the experiment. Alex Dioso (APL-UW) designed and maintains the data server. Dan Clark (APL-UW) helped with buoy fabrication.

REFERENCES

[1] J. Thomson, "Wave breaking dissipation observed with SWIFT drifters," *Journal of Atmospheric and Oceanic Technology*, vol. 29, no. 12, pp. 1866–1882, 2013/01/03 2012.

[2] J. Thomson, E. A. D'Asaro, M. Cronin, E. Rogers, R. Harcourt, and A. Schcerbina, "Waves and the equilibrium range at Ocean Weather Station P," *J. Geophys. Res.*, vol. 118, pp. 1–12, 2013.

[3] M. Schwendeman, J. Thomson, and J. Gemmrich, "Wave breaking dissipation in a young wind sea," *J. Phys. Oceanogr.*, vol. 44, no. 1, pp. 104–127, 2014.

[4] J. Thomson and W. E. Rogers, "Swell and sea in the emerging Arctic Ocean," *Geophysical Research Letters*, pp. n/a–n/a, 2014. [Online]. Available: http://dx.doi.org/10.1002/2014GL059983

[5] S. Zippel and J. Thomson, "Air-sea interactions in the marginal ice zone," *Elem Sci Anth*, vol. 4, no. 000095, 2016.

[6] S. F. Zippel, J. Thomson, and G. Farquharson, "Turbulence from breaking surface waves at a river mouth," *Journal of Physical Oceanography*, vol. 48, no. 2, pp. 435–453, 2018. [Online]. Available: https://doi.org/10.1175/JPO-D-17-0122.1

[7] P. Wiles, T. P. Rippeth, J. Simpson, and P. Hendricks, "A novel technique for measuring the rate of turbulent dissipation in the marine environment," *Geophys. Res. Let.*, vol. 33, p. L21608, 2006.

[8] A. Hay, L. Zedel, S. Nylund, R. Craig, and J. Culina, "The vectron a pulse coherent acoustic doppler system for remote turbulence resolving velocity measurements," in *Current, Waves and Turbulence Measurements (CWTM)*. IEEE/MTS, 2015.

[9] A. Y. Shcherbina, E. A. D'Asaro, and S. Nylund, "Observing finescale oceanic velocity structure with an autonomous nortek acoustic doppler current profiler," *Journal of Atmospheric and Oceanic Technology*, vol. 35, no. 2, pp. 411–427, 2018. [Online]. Available: https://doi.org/10.1175/JTECH-D-17-0108.1

[10] B. D. Scannell, T. P. Rippeth, J. H. Simpson, J. A. Polton, and J. E. Hopkins, "Correcting surface wave bias in structure function estimates of turbulent kinetic energy dissipation rate," *Journal of Atmospheric and Oceanic Technology*, vol. 34, no. 10, pp. 2257–2273, 2017.

[11] J. Thomson, Y. Fan, S. Stammerjohn, J. Stopa, W. E. Rogers, F. Girard-Ardhuin, F. Ardhuin, H. Shen, W. Perrie, H. Shen, S. Ackley, A. Babanin, Q. Liu, P. Guest, T. Maksym, P. Wadhams, C. Fairall, O. Persson, M. Doble, H. Graber, B. Lund, V. Squire, J. Gemmrich, S. Lehner, B. Holt, M. Meylan, J. Brozena, and J.-R. Bidlot, "Emerging trends in the sea state of the beaufort and chukchi seas," *Ocean Modelling*, vol. 105, pp. 1 – 12, 2016. [Online]. Available: http://www.sciencedirect.com/science/article/pii/S1463500316300622

[12] R. Pollard, "Interpretation of near-surface current meter observations," *Deep-Sea Research and Oceanographic Abstracts*, vol. 20, no. 3, pp. 261–268, 1973.

[13] M. J. Santala and E. A. Terray, "A technique for making unbiased estimates of current shear from a wave-follower," *Deep Sea Research Part A, Oceanographic Research Papers*, vol. 39, no. 3-4, pp. 607–622, 1992.

[14] R. Schudlich and J. Price, "Observations of seasonal variation in the Ekman layer," *Journal of Physical Oceanography*, vol. 28, no. 1993, pp. 1187–1204, 1998.

[15] N. Rascle and F. Ardhuin, "Drift and mixing under the ocean surface revisited: Stratified conditions and model-data comparisons," *Journal of Geophysical Research: Oceans*, vol. 114, no. 2, pp. 1–17, 2009.

[16] A. Amador, S. Jaramillo, and G. Pawlak, "ADCP bias and Stokes drift in AUV-based velocity measurements," *Journal of Atmospheric and Oceanic Technology*, vol. 34, no. 9, pp. 2029–2042, 2017.

[17] Ø. Breivik, P. a. E. M. Janssen, and J.-R. Bidlot, "Approximate Stokes Drift Profiles in Deep Water," *Journal of Physical Oceanography*, vol. 44, no. 9, pp. 2433–2445, 2014.

[18] N. Kumar, D. L. Cahl, S. C. Crosby, and G. Voulgaris, "Bulk versus Spectral Wave Parameters: Implications on Stokes Drift Estimates, Regional Wave Modeling, and HF Radars Applications," *Journal of Physical Oceanography*, vol. 47, no. 6, pp. 1413–1431, 2017.

[19] T. H. C. Herbers, P. F. Jessen, T. T. Janssen, D. B. Colbert, and J. H. MacMahan, "Observing ocean surface waves with GPS tracked buoys," *J. Atmos. Ocean. Tech.*, vol. 29, 2012.

[20] J. Thomson, J. B. Girton, R. Jha, and A. Trapani, "Measurements of directional wave spectra and wind stress from a wave glider autonomous surface vehicle," *Journal of Atmospheric and Oceanic Technology*, vol. 35, no. 2, pp. 347–363, 2018. [Online]. Available: https://doi.org/10.1175/JTECH-D-17-0091.1

[21] B. S. H. Connell, J. P. Rudzinsky, C. S. Brundick, W. M. Milewski, J. G. Kusters, and G. Farquharson, "Development of an environmental and ship motion forecasting system," in *Proceedings of the ASME 2015 34th International Conference on Ocean, Offshore and Arctic Engineering.*, 2015.

[22] J. A. Polton, D. M. Lewis, and S. E. Belcher, "The Role of Wave-Induced CoriolisStokes Forcing on the Wind-Driven Mixed Layer," *Journal of Physical Oceanography*, vol. 35, no. 4, pp. 444–457, 2005.

[23] A. J. Clarke and S. Van Gorder, "The Relationship of Near-Surface Flow, Stokes Drift and the Wind Stress," *Journal of Geophysical Research: Oceans*, pp. 1–13, 2018.

[24] A. J. Kuik, G. P. van Vledder, and L. H. Holthuijsen, "A Method for Routine Analysis of Pitch-and-Roll Buoy Wave Data," *Journal of Physical Oceanography*, vol. 18, pp. 1020–1034, 1988.

APPENDIX

Here we derive the bias in a velocity profile measured on a surface-wave-following drifter for intermediate waves, following the derivation for the deep-water case in Amador et al., 2017 [16]. Surface gravity wave horizontal and vertical velocities are given by

$$u_w = a\omega \frac{\cosh[k(z+h)]}{\sinh(kh)} \cos(kx - \omega t) \tag{13}$$

$$w_w = a\omega \frac{\sinh[k(z+h)]}{\sinh(kh)} \sin(kx - \omega t) \tag{14}$$

For a particle initially at position (X_0, Z_0) at time t = 0,

$$\tilde{u}(z) = a^2 \omega k \frac{\cosh[2k(Z_0+h) + k\Delta z]}{2\sinh^2(kh)} \tag{15}$$

A frequency-direction spectrum $S_{\eta\eta}(f,\theta)$ can be expressed as a product of a frequency spectrum, $S_{\eta\eta}(f)$, and a directional distribution at each frequency, $D_f(\theta)$:

$$S_{\eta\eta}(f,\theta) = S_{\eta\eta}(f) D_f(\theta) \tag{16}$$

The directional distribution can be expressed as a Fourier series

$$D_f(\theta_C) = a_1 \cos(\theta_C) + b_1 \sin(\theta_C) + a_2 \cos(2\theta_C) + b_2 \sin(2\theta_C) + a_3 \cos(3\theta_C) + b_3 \sin(3\theta_C) + ... \tag{17}$$

where $-1 < a_n < 1$ and $-1 < b_n < 1$ are the normalized directional Fourier coefficients and θ_C is a Cartesian angle (wave direction towards, counter-clockwise from east). The quantity $[a_n \cos(n\theta_C) + b_n \sin(n\theta_C)]$ is referred to as the n^{th} moment of the spectrum.

The coefficients a_1, b_1, a_2, and b_2 can be estimated from measurements with relative ease, as these coefficients can be related directly to the co- and quad-spectra of pressure and horizontal velocity components [24]. Higher-order moments usually cannot be estimated from measurements. The coefficients of the first and second moments can be used to estimate several statistical components of the spectrum without additional assumptions: mean direction (e.g., for use as a bulk wave parameter), directional spread, skewness, and kurtosis. The first four coefficients also can be used to constrain

a directional estimator that applies assumptions to estimate higher order moments.

Here, the coefficients a_1 and b_1 can be used to estimate the wave-following bias without using a directional estimator. These coefficients are related to the frequency-dependent directional distribution function as

$$a1 = \int D_f(\theta_C)\cos(\theta_C)d\theta_C \tag{18}$$

$$b1 = \int D_f(\theta_C)\sin(\theta_C)d\theta_C \tag{19}$$

Equation 5 results from substituting Equation 16 into Equation 6, and applying the definitions of a_1 and b_1 (Equations 18 and 19). At this order of Stokes drift, Equation 5 is an exact expression that accounts for both the wave direction (ratio of a_1 and b_1) and spread (a_1 and b_1 are smaller for larger directional spread).